Journal of Power Sources 268 (2014) 225–232

Contents lists available at ScienceDirect

Journal of Power Sources

journal homepage: www.elsevier.com/locate/jpowsour

Pt–Sn/C catalysts prepared by sodium borohydride reduction for alcohol oxidation in fuel cells: Effect of the precursor addition order

F.E. López-Suárez [a, *], A. Bueno-López [b], K.I.B. Eguiluz [a], G.R. Salazar-Banda [a]

[a] Electrochemistry and Nanotechnology Laboratory, Research and Technology Institute/Processes Engineering Post-graduation – PEP, Universidade Tiradentes, Av. Murilo Dantas, 300, Aracaju, SE, Brazil
[b] MCMA Group, Department of Inorganic Chemistry, Faculty of Sciences, University of Alicante, Ap. 99, E-03080 Alicante, Spain

HIGHLIGHTS

- Pt–Sn/C catalysts for ethanol oxidation synthesized modifying precursor addition order.
- The addition order of metals influences the physical–chemical properties of catalysts.
- Change in catalyst structure is directly related to activity during ethanol oxidation.
- Pt_3–Sn_1 catalyst prepared by co-precipitation of both metals shown the best performance.

ARTICLE INFO

Article history:
Received 19 March 2014
Received in revised form
6 June 2014
Accepted 7 June 2014
Available online 16 June 2014

Keywords:
Platinum
Tin
Ethanol oxidation reaction
Electrocatalysis
Fuel cell

ABSTRACT

A series of Pt–Sn/C catalysts used as anodes during ethanol oxidation are synthesized by a deposition process using $NaBH_4$ as the reducing agent. The order in which the precursors are added affects the electrocatalytic activity and physical–chemical characteristics of the bimetallic catalysts, where the Pt–Sn catalyst prepared by co-precipitation of both metals functions best below a potential of 0.5 V and the catalyst prepared by sequential deposition of Sn and Pt (drying after Sn addition) is most active above a potential of 0.5 V. The electrochemical behavior of catalysts during ethanol oxidation in an acidic medium are characterized and monitored in a half-cell test at room temperature by cyclic voltammetry, chronoamperometry and anode potentiostatic polarization. Catalyst structure and chemical composition are investigated by transmission electron microscopy (TEM), X-ray powder diffraction (XRD) and X-ray photoelectron spectroscopy (XPS). This behavior presented for best Pt–Sn catalyst can be attributed to the so-called bifunctional mechanism and to the electronic interaction between Pt and Sn.

1. Introduction

Fuel cells can produce electric energy directly from the oxidation of chemical products, and fuel cells using alcohols (direct alcohol fuel cells or DAFC) are attractive as power sources for mobile, stationary and portable applications [1–4]. Alcohols (mainly methanol) are possible fuels for mobile applications, and the direct oxidation of methanol in fuel cells has been widely investigated [5–8]. Wang et al. [9] found that ethanol serves as an alternative fuel, having an electrochemical activity comparable to methanol. Among alternative fuels, ethanol is a promising candidate since it can be readily produced from renewable sources and is less toxic than methanol [8].

The high activity and stability of Platinum metal, especially in acidic environments, makes it a suitable catalyst for electro-oxidation of many small organic molecules. However, in the case of ethanol, complete oxidation to CO_2 is more difficult (than methanol) due to the C–C bond cleavage and the strong adsorption of reaction intermediates which poison the Pt anode [10,11]. In this context, it is of great importance to develop anode catalysts for ethanol electrooxidation with greater activity than pure Pt to improve the performance of a direct ethanol fuel cell.

Efforts to mitigate Pt poisoning have been concentrated on the addition of co-catalysts, particularly Ru and Sn [1,12–24] as well as Pb, Sb, Rh, Mo, Os and Ir [23,25], while ternary Pt–Ru–Sn catalysts have been also recommended as suitable materials [15]. Among various Pt-based binary catalysts, Pt–Sn supported by carbon materials (Pt–Sn/C) [1,8,11,12,21,26–28] are effective during the

* Corresponding author. Tel.: +55 079 3218 2115; fax: +55 079 32182190.
E-mail addresses: franzedwin@gmail.com (F.E. López-Suárez), agus@ua.es (A. Bueno-López), katlin.eguiluz@pq.cnpq.br (K.I.B. Eguiluz), gianrsb@gmail.com (G.R. Salazar-Banda).

http://dx.doi.org/10.1016/j.jpowsour.2014.06.042
0378-7753/

electrooxidation of ethanol in an acid environment, which directly contrasts with the oxidation of methanol, where the most effective catalysts are Pt–Ru/C systems [1,29].

As for methanol oxidation, the superior performance of these binary electrocatalysts during ethanol oxidation when compared to pure Pt is attributed to the bifunctional effect (promoted mechanism) [30] and the electronic interaction between Pt and other metals in the alloy (intrinsic mechanism) [31]. For the promoted mechanism, the oxidation of strongly-adsorbed oxygen-containing species is facilitated by the presence of tin oxides which supply oxygen atoms to an adjacent site at a lower potential than pure Pt. The intrinsic mechanism postulates that Sn modifies the electronic structure of Pt, and as a consequence, the adsorption of oxygen-containing species.

The activity-promoting effect of Sn on Pt catalysts has been controversial, and diverse viewpoints have focused on the effects of either alloying Sn with Pt or adding SnO_2 to improve catalytic activity. Delime et al. [17] prepared bimetallic non-alloyed Pt–Sn catalysts and observed the presence of non-alloyed Sn led to increased current densities during the electrooxidation of ethanol. Jang et al. [32] compared the catalytic activity of a partially-alloyed Pt–Sn catalyst with that of a quasi-non-alloyed Pt–SnO_x catalyst, where the Pt–SnO_x catalyst shows higher catalytic activity during ethanol electrooxidation than the Pt–Sn alloy. The authors suggest the unchanged lattice parameter of Pt in the Pt–SnO_x catalyst is favorable to ethanol adsorption, and the tin oxide present in the vicinity of Pt nanoparticles could provide active oxygen species to remove the CO-like ethanolic residues and clean the Pt active sites.

Preparation procedures and Pt:Sn atomic ratios influence the performance of Pt–Sn/C electrocatalysts [11,12,26]. Lamy et al. [18,33,34] suggest an optimum composition for Sn in the 10–20 mol % range for catalysts prepared by a co-impregnation-reduction method. Zhou et al. [22] report the optimum composition is 33–40 mol % of Sn depending on the DAFC operation temperature. Jiang et al. [20] show that Pt–Sn/C electrocatalysts with Pt:Sn molar ratios of 66:33, 60:40 and 50:50 were more active than electrocatalysts with 75:25 and 80:20 M ratios. Spinacé et al. [35] investigated the activity of Pt–Sn/C electrocatalysts with varied Sn contents during ethanol oxidation using cyclic voltammetry, where the optimum Sn content in the catalyst depended upon the ratio between alloyed and non-alloyed Sn.

The physical–chemical properties of Pt–Sn electrocatalysts can be controlled by the preparation method. Lamy et al. [18,33] and Xin et al. [32,35] investigated ethanol oxidation using carbon-supported Pt–Sn catalysts prepared by a co-impregnation reduction method [18] and a modified polyol process [36], while Bonnemann et al. [37,38] developed a colloidal method to prepare unsupported and supported metals, which were then used to prepare carbon-supported fully non-alloyed Pt–Sn catalysts. Liu et al. [39] prepared carbon-supported Pt–Sn nanoparticles by a microwave-heated polyol process and Kim et al. [40] synthesized Pt–Sn/C catalysts using a borohydride reduction method followed by freeze-drying without heat treatment.

The methods developed by both Liu et al. [39] and Kim et al. [39,40] result in the formation of small and uniform Pt–Sn nanoparticles highly-dispersed on the carbon support. Carbon-supported catalysts can also be formed by the reduction of precursors with formic acid [19]. Others structures of Pt-based intermetallic and core/shell nanoparticles such as Pt/Sn are gaining attention due to their performance in many chemical and electrochemical reactions [41]. Silva et al. [12] carried out a systematic study of the formation of core–shell SnO_2@Pt/C structures using a novel preparation method based on a salt reduction process.

As the physical–chemical properties and electrocatalytic activity of these catalysts during ethanol oxidation depend on the synthesis method, this study investigated the effect of Pt and Sn addition order during the synthesis of Pt–Sn/C catalysts by a deposition process using $NaBH_4$ as the reducing agent. The catalysts were characterized by transmission electron microscopy (TEM), X-ray powder diffraction (XRD) and X-ray photoelectron spectroscopy (XPS), while the electrocatalytic behavior of these catalysts during ethanol oxidation in acid medium were studied by cyclic voltammetry, chronoamperometry and quasi-stationary potentiostatic polarization.

2. Experimental

2.1. Preparation of catalysts

The carbon support used was carbon black N330 (Alfa Aesar) with a BET area of 75 m^2 * g. The catalysts consisted of 20% (w/w) metal (Pt + Sn) on carbon with a nominal Pt:Sn molar ratio of 3:1, where the addition order of several metal precursor was studied:

i) Pt_3@Sn_1: Sequential reductive deposition, first adding Sn and then Pt.
ii) Pt_3@Sn_1-Intermediate: Prepared as for i, but dried after the addition of Sn.
iii) Pt_3–Sn_1: Both metals co-precipitated.
iv) Pt/C: Synthesized as for iii in the absence of Sn and used as the reference material.

Catalysts were synthesized by a deposition method using $NaBH_4$ as the reducing agent based on the procedure of Kaplan et al. [6]. The carbon support was added to 0.4 M HCl + $SnCl_2 \cdot 3H_2O$ and/or $H_2PtCl_6 \cdot 6H_2O$ solutions and stirred for 2 h. An ammonia solution was added while stirring until pH 11 was achieved, and an aqueous solution of $NaBH_4$ added to force the reduction and precipitation of the Pt and/or Sn metal cations. The mixture was stirred for 2 h, the powder recovered by filtration, washed with ultrapure water until no chloride ions could be detected and dried at 60 °C. The powder was washed with 0.5 M H_2SO_4 at 60 °C for 4 h to remove unstable moieties from the surface and yield a stable catalyst. All chemicals were analytically pure and used as received (Sigma Aldrich, purity >98%).

2.2. Catalysts characterizations

The crystalline structure was determined by X-ray diffraction in a Seifert powder diffractometer using CuK_α radiation (0.15418 nm). The diffractograms were registered at 2θ angles from 20 to 80°, with a step of 0.02° and a time per step of 3 s. The working conditions of the powder diffractometer were 1600 kW, a tension of 40 kV and a current of 40 mA.

XPS characterization was carried out in a VG-Microtech Multilab 3000 electron spectrometer using a Mg-K_α (1253.6 eV) radiation source. To obtain the XPS spectra, the pressure of the analysis chamber was maintained at $5 \cdot 10^{-10}$ mbar and the binding energy (BE) scale was adjusted by setting the C1s transition to 284.6 eV.

Transmission electron microscopy images were obtained using a JEOL (JEM-2010) microscope at 200 kV. A few droplets of an ultrasonically-dispersed suspension of each catalyst in ethanol were deposited on a copper grid with lacey carbon film and dried at ambient conditions for TEM characterizations. Particle size distributions were based upon ~200 particles for each catalyst.

2.3. Electrochemical measurements

Electrochemical measurements were performed at room temperature using an Autolab Model PGSTAT 30 potentiostat/

galvanostat. Experiments were carried out in a glass cell (one compartment) using a conventional three-electrode configuration (half-cell), and Boron-doped diamond (BDD) electrodes, prepared by the Centre Suisse d'Electronique et de Microtechnique SA (CSEM), Neuchâtel, were used as substrates for the electrocatalytic materials [42]. The boron content was ~800 ppm and the area of the working electrode exposed to the solution was 0.075 cm^2. The reference system consisted of a hydrogen electrode in the same solution (HESS) connected by a Luggin capillary, and a Pt coil (0.5 cm^2) was used as the counter-electrode. All potentials were referred to the reversible hydrogen electrode (RHE). Nitrogen gas was bubbled through all solutions for 15 min before starting each electrochemical test.

The catalyst ink was prepared by mixing 8 mg catalyst powder, 1 ml water (Milli-Q system) and 200 μl Nafion® solution (5 wt.% Aldrich solution), which was dispersed in an ultrasonic bath. The catalyst suspension (40 μl, 3.6 μg_{metal} cm^{-2}) was transferred with an injector to a BDD electrode and the electrode heated at 60 °C for 10 min.

Electrochemical activity tests were performed in aqueous 0.5 M H_2SO_4 solutions containing (a) 0.5 M C_2H_5OH, (b) 0.25 M CH_3CHO or (c) 0.25 M CH_3COOH at room temperature. Cyclic voltammetry experiments were performed between 0.0 and 0.8 V (*vs.* RHE) until stationary responses were obtained, then two voltammetric cycles were performed between 0.0 and 1.3 V (*vs.* RHE) at a scan rate of 0.02 V s^{-1} to evaluate the behavior of each electrocatalyst. Chronoamperometric experiments were performed at 0.5 V and 0.6 V (*vs.* RHE) and anode polarization curves obtained between 0.2 and 0.8 V (*vs.* RHE) in the potentiostatic mode, with all data points obtained after 200 s of polarization at each potential.

3. Results and discussion

3.1. Physical-chemical characterization of electrocatalysts

3.1.1. XRD characterization

Catalyst X-ray powder diffraction patterns are shown in Fig. 1. X-ray diffractograms showed two bands at 26° and 44°, assigned to the (002) and (100) planes of the graphite-like crystalline structure of the carbon support, respectively. The diffraction peaks at 2θ of 39.9°, 46.5° and 67.8° were assigned to the Pt (111), (200), and (220) planes, respectively (see JCPDS 04-0802 reference included in Fig. 1), which represented the typical character of a polycrystalline Pt-face centered cubic (fcc). Peaks of pure Sn or Sn oxides were not found, though their presence in small amounts or in an amorphous form cannot be discounted.

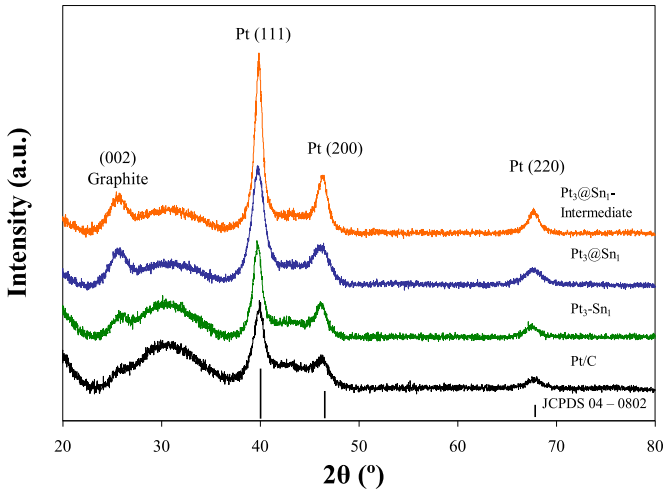

Fig. 1. X-ray diffractograms of samples.

The Pt (220) peak broadening was used to calculate the average particle size according to Scherrer's equation. The average particle size and lattice parameter are given in Table 1 which shows ~5.0–7.2 nm Pt–Sn particles were produced. The diffraction peaks of the Pt_3–Sn_1 catalyst were shifted to lower 2θ values with respect to the position of the Pt/C peaks, due to the formation of a $Pt_{1-x}Sn_x$ alloy with a lattice parameter <0.40 nm and $x = 0.3$, while some SnO_x was expected to remain as a segregated phase.

Pt and Sn can form five bimetallic intermetallic phases with molar ratios of Pt_3Sn, PtSn, Pt_2Sn_3, $PtSn_2$, and $PtSn_4$, which are distinguished by distinct crystalline structures [43], where Pt_3Sn and PtSn are congruently melting compositions. The shifts in the fcc Pt peaks for Pt–Sn/C catalysts to lower angles (with respect to those of pure Pt) should reveal the formation of a solid solution between Pt and Sn due to the incorporation of Sn in the fcc structure of Pt. In the cases of the $Pt_3@Sn_1$ and $Pt_3@Sn_1$-Intermediate catalysts, the positions of the Pt peaks were almost equal to the Pt/C position, which suggested that Sn was not incorporated into the cubic Pt lattice and that segregated phases should be formed, which was confirmed by the lattice parameters shown in Table 1. The lattice parameter of the Pt_3–Sn_1 catalyst was slightly higher than Pt/C, indicating lattice expansion due to alloying. The lattice parameter values were almost equal for $Pt_3@Sn_1$-Intermediate, $Pt_3@Sn_1$ and Pt/C, showing the preparation method did not change the crystal structure of Pt.

The sharp peaks presented by $Pt_3@Sn_1$-Intermediate could be due to the formation of a Pt_{shell}–SnO_{2core}/C core–shell structure. The lattice parameter of Pt on $Pt_3@Sn_1$-Intermediate was 0.3910 nm, which was slightly compressed compared with that of pure Pt at 0.3915 nm. The shifted position to higher angles compared with bulk Pt, and the relatively strong Pt (111) diffraction peak, was consistent with a compressed lattice. Monometallic Pt nanoparticles synthesized under identical conditions indicated bulk Pt diffraction patterns did not show anomalies in their peak positions. As the Pt shell becomes thicker with further overlayers, the peak positions for the (111) diffraction shift to their 'normal' position with increasing intensities [44].

3.1.2. TEM characterization

TEM micrographs and histograms of the catalysts are shown in Fig. 2a–d, where small black Pt particles were dispersed on the carbon support and aggregates were also seen. The formation of aggregates appeared to be favored by the addition of Sn, since they were not seen on the Pt/C reference catalyst. The average sizes of the particles obtained by TEM (inset in Fig. 2 and data in Table 1) agreed with values calculated from XRD patterns.

3.1.3. XPS characterization

XPS analysis provided information about catalyst surface composition. The XPS survey analysis of the catalysts (survey of $Pt_3@Sn_1$-Intermediate is included in Fig. 3 as an example) indicated that sodium and boron were present on the catalyst surface due to

Table 1
Structural characteristic obtained from XRD and TEM.

Catalyst	Particle size (nm)[a]	Lattice parameter (nm)	Average particle size from TEM (nm)
Pt/C	7.2	0.3915	8.5 ± 2.1
$Pt_3@Sn_1$	6.2	0.3913	5.4 ± 1.8
Pt_3–Sn_1	5.3	0.3926	6.0 ± 0.9
$Pt_3@Sn_1$-Intermediate	5.0	0.3910	6.7 ± 2.4

[a] Calculated from Pt (220) peak with the Scherrer's formula.

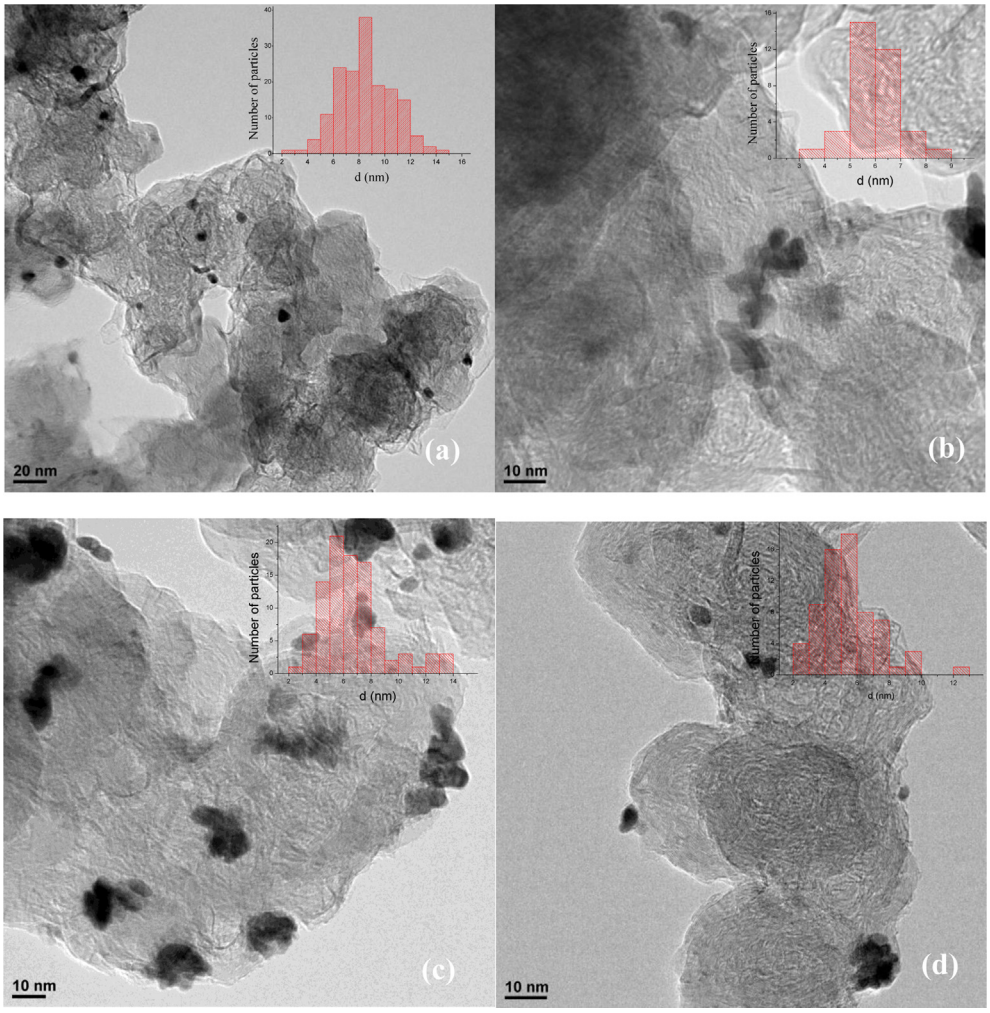

Fig. 2. TEM images of Pt/C (a), Pt_3–Sn_1 (b), Pt_3@Sn_1 (c) and Pt_3@Sn_1-Intermediate (d) catalysts.

$NaBH_4$ being used as the reducing agent, while chlorine was not detected. The oxidation states of Pt and Sn were studied by XPS following the Pt 4f and Sn 3p transitions, respectively. The Pt 4f spectral profiles for Pt–Sn/C catalysts are included in Fig. 4, where

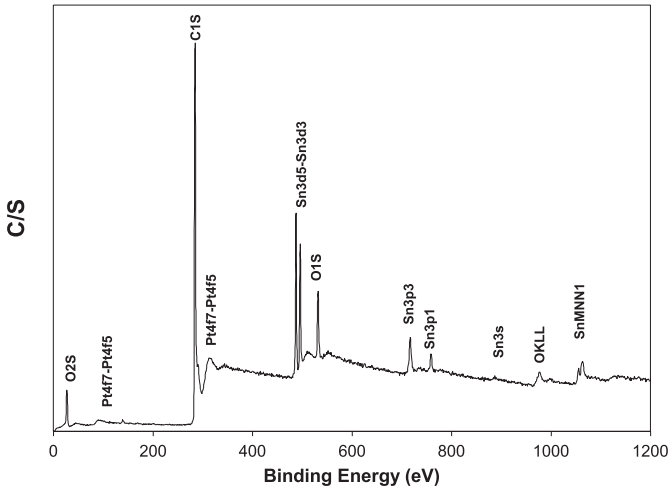

Fig. 3. XPS survey analysis of the Pt_3@Sn_1-Intermediate catalyst.

the Pt 4f region displayed spin-orbital splitting of the $4f_{7/2}$ and $4f_{5/2}$ states. In Fig. 4, the maximum energies of the main bands for all samples appeared at 71.6 eV and 74.8 eV, suggesting the presence of metallic Pt, and the binding energy values for metallic Pt were in agreement with published data [45]. In order to identify higher Pt oxidation states, the broad profiles could be deconvoluted into four different peaks with maxima at 71.6, 72.6, 74.8 and 75.7 eV, which corresponded to different oxidation states of Pt. The deconvoluted peaks centered at 72.6 and 75.7 eV could be attributed to the Pt^{2+} and Pt^{4+}species, respectively [46], while those at 71.6 and 74.8 eV were attributed to metallic Pt. The binding energy of the metallic Pt peaks (71.6 eV) was slightly higher than typical values reported in the literature (70.7–71.1 eV) [47], which could be explained by the small particle size of Pt or by the formation of an alloy with Sn [48]. This shift in binding energy with regard to pure Pt has also been attributed to Pt-support interactions such as those seen for carbon- or zeolite-supported Pt [49–51].

The binding energies of metallic Pt for Pt_3–Sn_1 and Pt_3@Sn_1 (71.3 and 74.6 eV), as well as Pt_3@Sn_1-Intermediate (71.2 and 74.4 eV), were slightly lower than those of Pt/C (71.6 and 74.8). These XPS data indicated the electronic structure of Pt was modified by Sn addition. Kim et al. [40] reported charge transfer from the less-electronegative Sn to the more-electronegative Pt.

Table 2 shows the percentage of Pt and Sn species calculated from the relative intensities of deconvoluted peaks and Pt/Sn

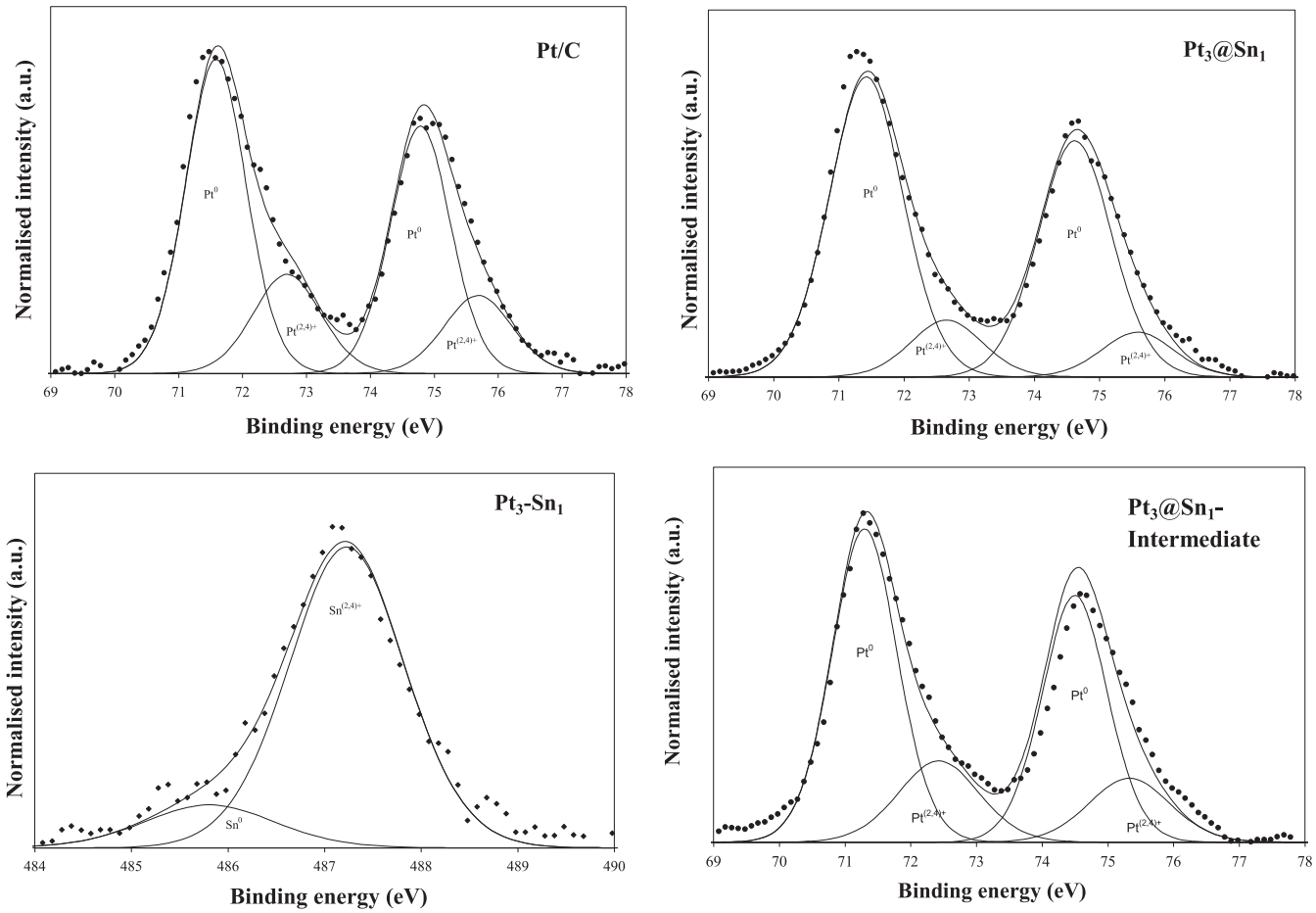

Fig. 4. Pt 4f transition in XPS experiments performed with catalysts.

surface composition observed from the XPS results. The areas under the different deconvoluted Pt peaks were quantified for all catalysts and the corresponding percentages calculated as a function of the total area. The results showed a prevailing presence of metallic Pt on the catalyst surface (between 75 and 84%) for all samples studied, while the fraction of oxidized Pt species (15–25%) could be formed during catalyst exposure to the atmosphere.

Fig. 5 shows the Sn $3d_{5/2}$ signal deconvoluted into two different peaks. The Pt_3–Sn_1 catalyst had a low binding energy peak centered at 485.8 eV, which was attributed to metallic Sn, and a primary high binding energy peak at 487.1–487.4 eV assigned to Sn^{4+} species [47]. For Pt_3@Sn_1-Intermediate and Pt_3@Sn1 catalysts, a small peak attributed Sn^0 was observed, as the majority of the tin was oxidized (see, Table 2). The higher fraction of metallic Sn observed on Pt_3–Sn_1, which was in agreement with the formation of a metallic Pt–Sn alloy indicated by XRD, could explain the improved interaction with Pt.

Table 2
Percentage of different Pt species observed from the XPS data.

Catalyst	Pt(0)/Pt(II) species (%)	Sn (0)/Sn (IV) species (%)	Surface Pt/Sn composition (%)	Nominal Pt/Sn composition (%)
Pt/C	74/26		13/0	20/0
Pt_3@Sn_1	84/16	4/96	10/2	16.7/3.3
Pt_3–Sn_1	81/19	15/85	18/7	16.7/3.3
Pt_3@Sn_1-Intermediate	76/24	3/97	11/7	16.7/3.3

3.2. Electrochemical characterization

Fig. 6 shows cyclic voltammograms obtained in 0.5 M H_2SO_4 at a scan rate of 0.02 V s^{-1} (all catalysts), which indicated the typical behavior of the hydrogen and oxide regions of Pt in the materials when in acid solutions [52]. The adsorption/desorption of hydrogen between 0.05 and 0.4 V (*vs.* RHE) was seen for all catalysts, but this zone was not well-defined. In the case of the Pt_3–Sn_1 catalyst, a large value for double-layer charging current (0.4–0.8 V) was seen, attributed to the presence of tin oxides on the particle surface that increase electrode capacitance [52]. The hydrogen-desorption region for Pt_3–Sn_1 was modified in comparison to Pt_3@Sn_1, Pt_3@Sn_1-Intermediate and Pt/C, which could indicate there were less Pt species on the surface of this catalyst. Based on these data, the structure of peaks in the electrochemical profiles appeared to depend predominantly on the preparation method.

The electrocatalytic activities of the different catalysts during the oxidation of ethanol were compared by cyclic voltammetry, chronoamperometric and quasi-steady-state polarization measurements at room temperature. Fig. 7 shows the anodic scan of the cyclic voltammetries for the different electrocatalysts, and the inset in Fig. 7 shows the higher overpotential regions in detail. At overpotentials below 0.5 V, the profiles indicated lower and similar electrocatalytic activities for Pt_3@Sn_1, Pt_3@Sn_1-Intermediate and Pt/C. This behavior is due to dissociative adsorption and dehydrogenation of ethanol that leads to coverage active surface sites of Pt with intermediates products. The Pt_3–Sn_1 catalyst shown the best performance since the onset of ethanol oxidation occurs at 0.26 V.

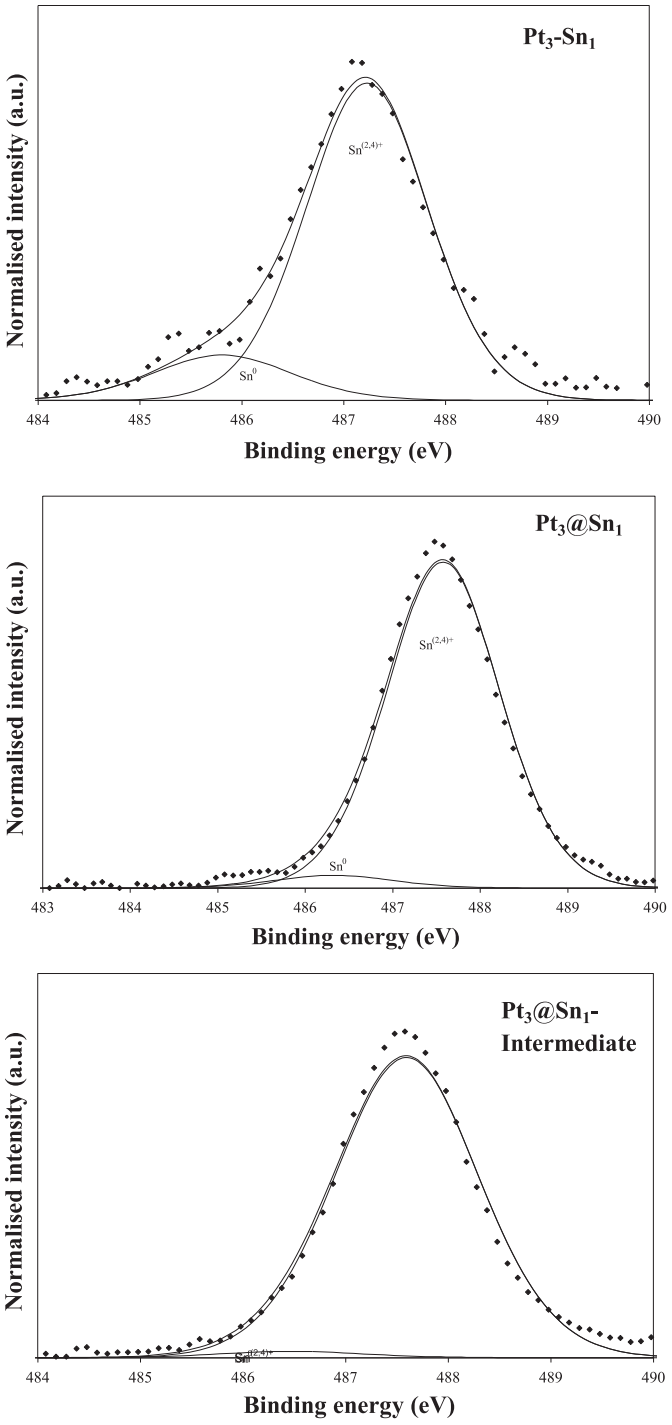

Fig. 5. Sn 3d transition in XPS experiments performed with catalysts.

At high overpotentials, Pt/C showed a higher current density. Cyclic voltammetry results showed that Pt_3—Sn_1 was a more suitable electrocatalyst for ethanol oxidation (compared to other catalysts studied here) because the energy necessary for ethanol electrooxidation was lower.

All catalysts displayed a single oxidation peak during the forward sweep process in the studied potential range (Fig. 7), and the oxidation peak during the backward sweep process (Fig. 1S, Supporting information) could be attributed to further oxidation of the adsorbed intermediate species of ethanol. For the Pt/C

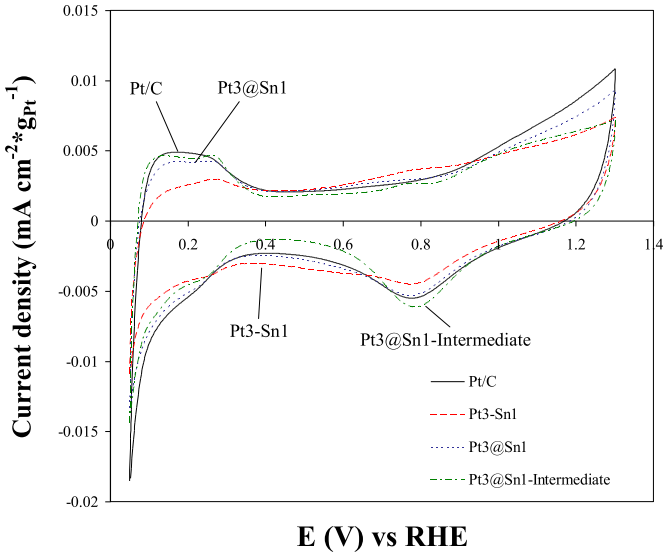

Fig. 6. Cyclic voltammetry curves for electrocatalysts in 0.5 M H_2SO_4 electrolyte. Scan rate of 0.02 V s^{-1}.

catalyst, this backward oxidation peak was higher for Sn-containing catalysts, which was attributed to the promoting role of Sn in the oxidative removal of the adsorbed ethanol oxidation intermediate species (with respect to Pt).

Chronoamperometric curves were recorded at 0.5 V and 0.6 V (*vs.* RHE) (Fig. 8a and b, respectively) to compare the catalytic activity of the anode catalysts. During the first seconds, there was a sharp decrease in the current density followed by a slow decrease in the current density values for longer time periods, and a steady-state current observed for all catalysts after ca. 200 s. The test at 0.5 V corroborated the higher activity of the Pt_3—Sn_1 catalyst in comparison to other catalysts, whereas similar behaviors for the Pt_3—Sn_1 and Pt_3@Sn_1-Intermediate catalysts were seen at 0.6 V.

Fig. 9 shows anode polarization curves. The onset potential of ethanol electrooxidation using Pt_3—Sn_1 was shifted negatively by ~0.2 V in comparison to Pt/C, and by 0.1 V for Pt_3@Sn_1 and Pt_3@Sn_1-Intermediate. Below 0.6 V, Pt_3—Sn_1 showed the highest current

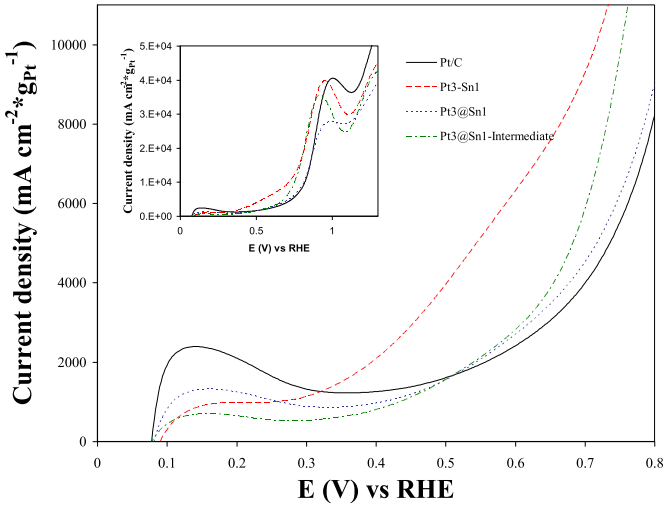

Fig. 7. Anodic sweep of the cyclic voltammetry recorded for ethanol oxidation in the 0.50 M C_2H_5OH/0.5 M H_2SO_4 solution. Scan rate of 0.02 V s^{-1}. Inset: detail of the high potential region.

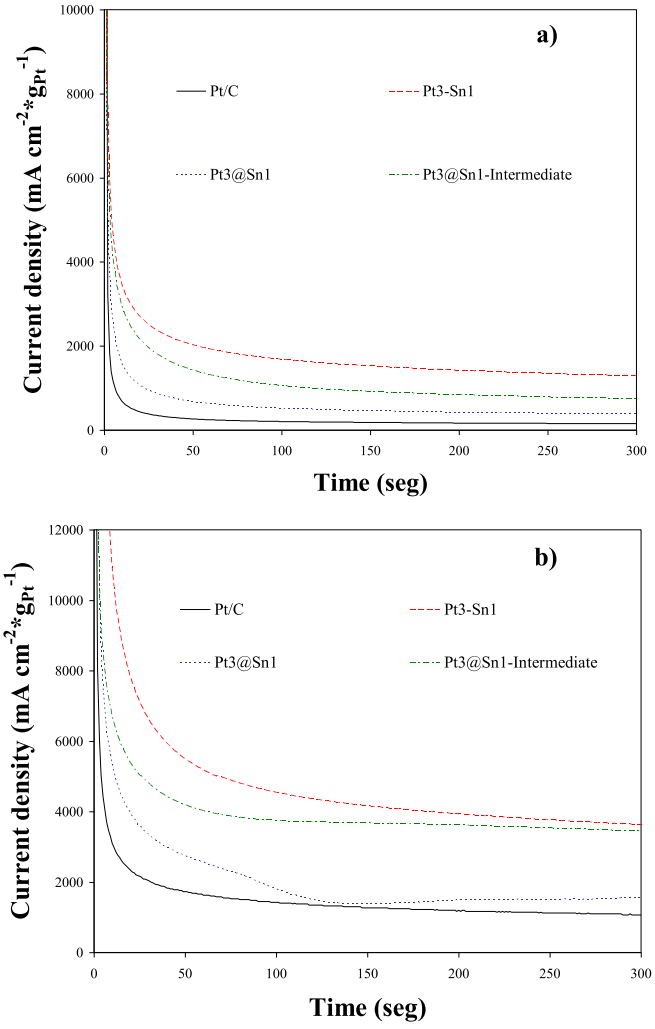

Fig. 8. Chronoamperometric curves for the oxidation of ethanol in 0.5 M C_2H_5OH/0.5 M H_2SO_4 solution at 0.5 V (a) and 0.6 V (b) *versus* RHE.

density, while at 0.6 V and above, the $Pt_3@Sn_1$-Intermediate catalyst had the highest activity.

Studies on the electrooxidation of ethanol have identified adsorbed intermediates present on Pt–Sn/C catalysts, which consist primarily of partial oxidation products like CH_3CHO and CH_3COOH [53]. Electrooxidation tests of CH_3CHO and CH_3COOH were carried out for the best catalyst Pt_3–Sn_1 and with $Pt_3@Sn_1$-Intermediate and Pt/C as reference. The anodic scans of the cyclic voltammetries for CH_3CHO are presented in Fig. 10. When Pt_3–Sn_1 was used, the activity of ethanol electrooxidation (see, Fig. 7) and the activity for the oxidation of its intermediate products (acetaldehyde, Fig. 10) were higher than those for $Pt_3@Sn_1$-Intermediate and Pt/C. Generally, in the case of ethanol and acetaldehyde electrooxidation, enhanced activity could be reflected in the form of a negatively-shifted onset potential and increased current density. The $Pt_3@Sn_1$-Intermediate catalyst was only active at a high potential (>0.8 V) while the Pt/C catalyst showed lower activity. Finally, the Pt–Sn/C catalysts prepared in this study did not show CH_3COOH electrooxidation activity, which is in agreement with the inhibition of the C–C bond cleavage reactions reported for Pt–Sn catalysts [1].

The negative potential shift at the beginning of ethanol oxidation using the Pt_3–Sn_1 catalyst could be attributed to the synergistic activities of Sn and Pt (promoted mechanism) for ethanol electrooxidation and to the structural modification of Pt by Sn doping (intrinsic mechanism). The results at a higher potential (>0.6 V) indicated the best catalyst was the $Pt_3@Sn_1$-Intermediate catalyst, due to the electronic interaction in the Pt_{shell}–SnO_{2core}/C structure. For the $Pt_3@Sn_1$ catalyst, a possible reason for lower activity could be the formation of isolated Pt and SnO_2 particles and/or blockage of Pt active sites (higher time reduction of Sn than Pt particles is necessary) that did not allow a cooperative effect between Pt and Sn particles.

4. Conclusions

Data indicated modification of metal precursor addition order influenced the physical–chemical properties of the Pt–Sn catalyst. The Pt and Sn species present on the catalyst surface could be: i) partially alloyed $Pt_{1-x}Sn_x$, with $x = 0.3$ and SnO_x for the Pt_3–Sn_1catalyst, ii) Pt_{shell}–SnO_{2core}/C and SnO_x particles for $Pt_3@Sn_1$ and iii) Pt–SnO_x or Sn adatom modified Pt for the $Pt_3@Sn_1$-

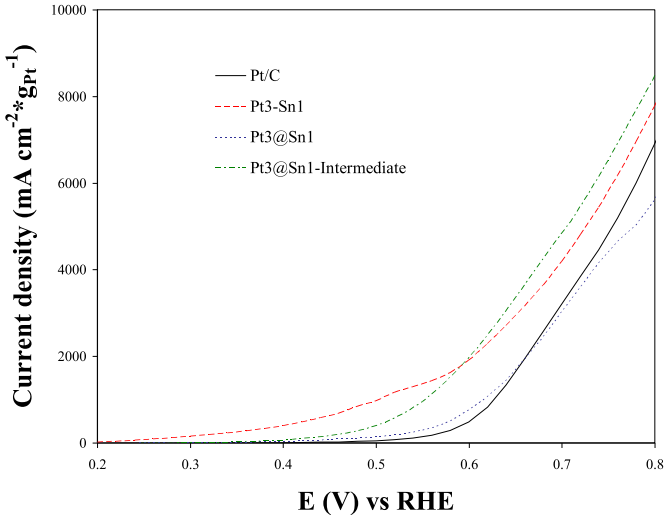

Fig. 9. Anode polarization profiles for the oxidation of ethanol in 0.50 M C_2H_5OH/0.5 M H_2SO_4 solution.

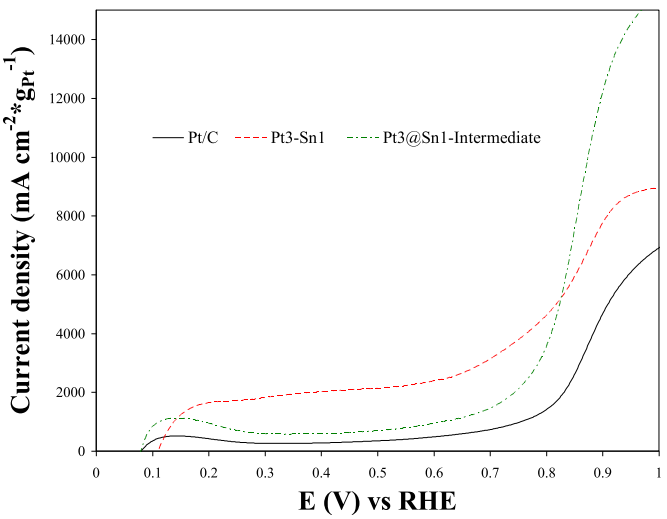

Fig. 10. Anodic sweep of the cyclic voltammetry recorded for acetaldehyde oxidation in the 0.50 M CH_3CHO/0.5 M H_2SO_4 solution.

Intermediate catalyst. This change in catalyst structure was directly related to the electrocatalytic activity during ethanol oxidation. At potentials below 0.6 V, Pt_3–Sn_1 showed the best activity for ethanol and acetaldehyde electrooxidation, which could be attributed to the synergistic interactions between Sn and Pt catalytic activities and the structural modification of Sn by Pt (intrinsic mechanism). Pt_3@Sn_1-Intermediate displayed the highest catalytic activity above 0.6 V, which was due to the electronic interactions in the Pt_{shell}–SnO_{2core}/C, where Sn could decrease the formation of cationic Pt species and promote the formation of free Pt metal active sites for ethanol chemisorption and the consequent dehydrogenation reaction. XRD, TEM and XPS results showed that Pt nanoparticles could be easily synthesized, even at a high metal loading, without the use of expensive surfactants.

Acknowledgments

The authors thank the Brazilian National Council of Technological and Scientific Development-CNPq (grants: 303630/2012-4, 402243/2012-9 and 310282/2013-6) for the scholarships and financial support for this work.

Appendix A. Supplementary data

Supplementary data related to this article can be found at http://dx.doi.org/10.1016/j.jpowsour.2014.06.042.

References

[1] E. Antolini, J. Power Sources 170 (2007) 1–12.
[2] B.C. Steele, A. Heinzel, Nature 414 (2001) 345–352.
[3] L. Schlapbach, A. Züttel, Nature 414 (2001) 353–358.
[4] L. Carrette, K. Friedrich, U. Stimming, Fuel Cells 1 (2001) 5–39.
[5] A. Arico, V. Baglio, A. Di Blasi, E. Modica, P. Antonucci, V. Antonucci, J. Electroanal. Chem. 557 (2003) 167–176.
[6] D. Kaplan, M. Alon, L. Burstein, Y. Rosenberg, E. Peled, J. Power Sources 196 (2011) 1078–1083.
[7] S. Kuk, A. Wieckowski, J. Power Sources 141 (2005) 1–7.
[8] C. Lamy, E. Belgsir, J. Leger, J. Appl. Electrochem. 31 (2001) 799–809.
[9] J. Wang, S. Wasmus, R. Savinell, J. Electrochem. Soc. 142 (1995) 4218–4224.
[10] S. Rousseau, C. Coutanceau, C. Lamy, J.-M. Léger, J. Power Sources 158 (2006) 18–24.
[11] E. Antolini, E. Gonzalez, Catal. Today 160 (2011) 28–38.
[12] J. Silva, R. De Souza, L. Parreira, E.T. Neto, M. Calegaro, M. Santos, Appl. Catal. B Environ. 99 (2010) 265–271.
[13] S. Song, C. He, J. Liu, Y. Wang, A. Brouzgou, P. Tsiakaras, Appl. Catal. B Environ. 119 (2012) 227–233.
[14] N. Fujiwara, K. Friedrich, U. Stimming, J. Electroanal. Chem. 472 (1999) 120–125.
[15] W. Zhou, W.Z. Li, S.Q. Song, Z.H. Zhou, L. Jiang, G. Sun, Q. Xin, K. Poulianitis, S. Kontou, P. Tsiakaras, J. Power Sources 131 (2004) 217–223.
[16] A. Neto, R. Verjulio-Silva, M. Linardi, E. Spinacé, Int. J. Electrochem. Sci. 4 (2009) 954–961.
[17] F. Delime, J. Leger, C. Lamy, J. Appl. Electrochem. 29 (1999) 1249–1254.
[18] F. Vigier, C. Coutanceau, A. Perrard, E. Belgsir, C. Lamy, J. Appl. Electrochem. 34 (2004) 439–446.
[19] F. Colmati, E. Antolini, E.R. Gonzalez, Appl. Catal. B Environ. 73 (2007) 106–115.
[20] L. Jiang, G. Sun, Z. Zhou, W. Zhou, Q. Xin, Catal. Today 93 (2004) 665–670.
[21] S. Zignani, E. Gonzalez, V. Baglio, S. Siracusano, A. Aricò, Int. J. Electrochem. Sci. 7 (2012) 3155–3166.
[22] W. Zhou, S. Song, W. Li, G. Sun, Q. Xin, S. Kontou, K. Poulianitis, P. Tsiakaras, Solid State Ionics 175 (2004) 797–803.
[23] S. Song, W. Zhou, Z. Zhou, L. Jiang, G. Sun, Q. Xin, V. Leontidis, S. Kontou, P. Tsiakaras, Int. J. Hydrogen. Energy 30 (2005) 995–1001.
[24] B. Braunchweig, D. Hibbitts, M. Neurock, A. Wieckowski, Catal. Today 2012 (2012) 197–209.
[25] X. Zhou, Y. Gan, J. Du, D. Tian, R. Zhang, C. Yang, Z. Dai, J. Power Sources 232 (2013) 310–322.
[26] F. Purgato, S. Pronier, P. Olivi, A. De Andrade, J. Léger, G. Tremiliosi-Filho, K. Kokoh, J. Power Sources 198 (2012) 95–99.
[27] Y. Wang, S. Song, G. Andreadis, H. Liu, P. Tsiakaras, J. Power Sources 196 (2011) 4980–4986.
[28] C. Lamy, A. Lima, V. LeRhun, F. Delime, C. Coutanceau, J.-M. Léger, J. Power Sources 105 (2002) 283–296.
[29] G. Camara, R. De Lima, T. Iwasita, Electrochem. Commun. 6 (2004) 812–815.
[30] K. Wang, H. Gasteiger, N. Markovic, P. Ross, Electrochim. Acta 41 (1996) 2587–2593.
[31] P. Christensen, A. Hamnett, G. Troughton, J. Electroanal. Chem. 362 (1993) 207–218.
[32] L. Jiang, G. Sun, S. Sun, J. Liu, S. Tang, H. Li, B. Zhou, Q. Xin, Electrochim. Acta 50 (2005) 5384–5389.
[33] C. Lamy, S. Rousseau, E. Belgsir, C. Coutanceau, J.-M. Léger, Electrochim. Acta 49 (2004) 3901–3908.
[34] A. Verma, S. Basu, J. Power Sources 145 (2005) 282–285.
[35] E.V. Spinacé, L.A. do Vale, R.R. Dias, A.O. Neto, M. Linardi, Stud. Surf. Sci. Catal. 162 (2006) 617–624.
[36] T. Iwasita, Electrochim. Acta 47 (2002) 3663–3674.
[37] H. Bönnemann, W. Brijoux, T. Joussen, Angew. Chem. Int. Ed. (Engl.) 29 (1990) 273–275.
[38] H. Bönnemann, W. Brijoux, R. Brinkmann, R. Fretzen, T. Joussen, R. Köppler, B. Korall, P. Neiteler, J. Richter, J. Mol. Catal. 86 (1994) 129–177.
[39] Z. Liu, B. Guo, L. Hong, T.H. Lim, Electrochem. Commun. 8 (2006) 83–90.
[40] J.H. Kim, S.M. Choi, S.H. Nam, M.H. Seo, S.H. Choi, W.B. Kim, Appl. Catal. B Environ. 82 (2008) 89–102.
[41] X. Wang, L. Altmann, J.r. Stöver, V. Zielasek, M. Bäumer, K. Al-Shamery, H. Borchert, J.r. Parisi, J. Kolny-Olesiak, Chem. Mater. 25 (2012) 1400–1407.
[42] G.R. Salazar-Banda, K.I. Eguiluz, M. Pupo, H.B. Suffredini, M.L. Calegaro, L.A. Avaca, J. Electroanal. Chem. 668 (2012) 13–25.
[43] V. Kuznetsov, A. Belyi, E. Yurchenko, M. Smolikov, M. Protasova, E. Zatolokina, V. Duplyakin, J. Catal. 99 (1986) 159–170.
[44] S. Alayoglu, A.U. Nilekar, M. Mavrikakis, B. Eichhorn, Nat. Mater. 7 (2008) 333–338.
[45] S. Hüfner, G. Wertheim, Phys. Rev. B 11 (1975) 678–683.
[46] S. Sun, D. Yang, D. Villers, G. Zhang, E. Sacher, J.-P. Dodelet, Adv. Mater. 20 (2008) 571–574.
[47] www.lasurface.com, in.
[48] M. Goetz, H. Wendt, J. Appl. Electrochem. 31 (2001) 811–817.
[49] E. Antolini, L. Giorgi, F. Cardellini, E. Passalacqua, J. Solid State Electrochem. 5 (2001) 131–140.
[50] J.C. Vedrine, M. Dufaux, C. Naccache, B. Imelik, J. Chem. Soc. Faraday Trans. 1 (74) (1978) 440–449.
[51] S.-G.P.P.-M. Oxide, Chem. Mater. 18 (2006) 5563–5570.
[52] D. Stevens, J.R. Dahn, J. Electrochem. Soc. 150 (2003) A770–A775.
[53] S.C. Chang, L.W.H. Leung, M.J. Weaver, J. Phys. Chem. 94 (1990) 6013–6021.